

Equation-of-state-insensitive measure of neutron star stiffness

Jayana A. Saes* and Raissa F. P. Mendes†

Instituto de Física, Universidade Federal Fluminense, Niterói, Rio de Janeiro, 24210-346, Brazil.

(Dated: August 30, 2022)

Universal relations (i.e., insensitive to the equation of state) between macroscopic properties of neutron stars have proven useful for a variety of applications—from providing a direct means to extract observables from data to breaking degeneracies that hinder tests of general relativity. Similarly, equation-of-state-insensitive relations directly connecting macroscopic and microscopic properties of neutron stars can potentially provide a clean window into the behavior of nuclear matter. In this work, we uncover a tight correlation between certain macroscopic properties of a neutron star—its compactness C , moment of inertia \bar{I} and tidal deformability $\bar{\Lambda}$ —and the ratio $\alpha_c \equiv p_c/\epsilon_c$ of central pressure to central energy density, which can be interpreted as a mean notion of the stiffness of nuclear matter inside that object. We describe interesting properties of this stiffness measure, quantify the (approximate) universality of the $\alpha_c - C/\bar{I}/\bar{\Lambda}$ relations, and explore its consequences in the face of recent and future neutron star observations.

I. INTRODUCTION

Different observational channels are nowadays converging to compose an increasingly clear picture of neutron stars (NSs). Radio observations of rotation-powered pulsars have enabled accurate mass measurements for the components of a number of binary systems (see, e.g. [1–3]), while pulse profile modeling of the x-ray data from the Neutron-Star-Interior-Composition Explorer (NICER) already provided measurements of the radius of two NSs [4–7], improving the accuracy of previous radii estimates. Additionally, observation of gravitational waves (GWs) from the binary NS merger GW170817 allowed a first measurement of the tidal deformability [8, 9], with its electromagnetic counterpart providing valuable information about the remnant [10]. Future years should witness the measurement of additional NS properties, such as their moment of inertia [11] or characteristic pulsation modes [12–14].

All of these observables depend on the nuclear equation of state (EOS), which, for a cold NS, consists of a one-parameter relation between pressure and rest-mass density, $p = p(\rho)$. At the supranuclear densities thought to exist in NS cores, the EOS is mostly unconstrained by nuclear physics experiments. As a result, different theoretical strategies to extrapolate nuclear physics models to this high density regime give rise to disparate predictions for NS properties [15, 16].

Interestingly, EOS-insensitive relations have been found to exist between several macroscopic NS observables (see e.g. [17] and references therein). These relations are particularly useful to break degeneracies that would otherwise hinder an accurate estimation of NS properties. For example, the “binary Love relation” [18, 19] between certain combinations of the tidal deformabilities of the components of a binary

system can be used to infer the individual deformabilities, which are not currently measurable in GW data. Moreover, EOS-insensitive relations make comparison between various measurements of NS properties more straightforward. For instance, one can use the Love- C [20, 21] relation, between the tidal deformability and the NS compactness, to translate a measurement of mass and tidal deformability—inferred from GW data—into an estimate of the NS radius, making comparison with other radius measurements (say, from NICER data) more direct. Some EOS-insensitive relations, such as those connecting moment of inertia, tidal deformability and quadrupole moment (“I-Love-Q”) are incredibly tight, holding to roughly percent accuracy [20].

EOS-insensitive relations have also been found, relating directly macroscopic and microscopic observables. For instance, pressure at ~ 1 -2 times the nuclear saturation density ($\rho_{\text{sat}} = 2.8 \times 10^{14} \text{ g cm}^{-3}$) was found to correlate with the radius and tidal deformability of a typical NS [22, 23], while pressure at higher densities (~ 7 -8 ρ_{sat}) is thought to determine their maximum mass [24]. Estimates for the pressure at fiducial densities, coming from NS observations, can then be fed into nuclear physics models, constraining properties of the nuclear interaction such as the nuclear symmetry energy [25, 26].

The aim of this work is to introduce and explore a new approximately universal relation between certain macroscopic NS properties and a microscopic measure of the mean stiffness of nuclear matter inside a NS, namely, the ratio $\alpha_c \equiv p_c/\epsilon_c$ of central pressure to central energy density. This stiffness measure harbors similarities with more commonly used notions, such as the maximum speed of sound inside a NS. However, it correlates much more strongly with macroscopic observables such as the NS compactness (C), dimensionless moment of inertia (\bar{I}) or tidal deformability ($\bar{\Lambda}$). The approximately universal $\alpha_c - C/\bar{I}/\bar{\Lambda}$ relations are analyzed in this work both for a restricted set of realistic EOS and for a larger set of $\sim 60,000$ phenomenological EOS, in two different EOS parametriza-

* jayanasaes@id.uff.br

† rfpmendes@id.uff.br

tions [27, 28]. Our main results are condensed in Figs. 3 and 4. As an example, the $\alpha_c - \bar{\Lambda}$ relation is found to hold to a maximum error of $\sim 8\%$ for the set of realistic EOS, and to a maximum error of $\sim 38\%$ for the set of (generalized) piecewise-polytropic EOS, with 90% of the error below $\sim 7\%$ in this case. Measurements of tidal deformability, moment of inertia or compactness can thus be translated into estimates for α_c , providing direct information about the behavior—and extremeness—of nuclear matter inside NSs.

This work is organized as follows. We begin in Sec. II by describing the properties and physical interpretation of the stiffness measure α_c . Section III contains the description of the set of realistic and phenomenological EOS used subsequently. Our main results for the approximate universality of the $\alpha_c - C/\bar{I}/\bar{\Lambda}$ relations are presented in Sec. IV, while Sec. V explores how present and future observations may constrain this microscopic quantity. Section VI gathers our main conclusions. We adopt natural units, $c = G = 1$, unless stated otherwise.

II. PROPERTIES OF THE STIFFNESS MEASURE

The stiffness of nuclear matter encodes how pressure increases as density increases. Commonly used measures include the adiabatic sound speed,

$$c_s = \sqrt{\left. \frac{\partial p}{\partial \epsilon} \right|_s} \quad (1)$$

and the adiabatic index,

$$\Gamma_1 = \left(\frac{\partial \ln p}{\partial \ln \rho} \right)_s, \quad (2)$$

where p , ϵ , ρ , and s are the fluid pressure, energy density, rest-mass density, and entropy as measured by comoving observers. Both c_s and Γ_1 are local stiffness measures: For each value of the energy density, $c_s^2(\epsilon)$ measures the slope of the $p(\epsilon)$ relation, and similarly for Γ_1 . On the other hand, one can think of the ratio

$$\alpha(\epsilon) \equiv \frac{p(\epsilon)}{\epsilon}, \quad (3)$$

when evaluated at the stellar center [$\alpha_c \equiv \alpha(\epsilon_c)$], as a global, or mean, notion of the stiffness of nuclear matter inside that NS. Indeed, since pressure vanishes at the stellar surface ($p_s = 0$) and $\epsilon_s/\epsilon_c \approx 0$, $\alpha_c \approx (p_c - p_s)/(\epsilon_c - \epsilon_s)$, the ratio between the total increase in pressure and the total increase in energy density from the surface to the center. This is illustrated in Fig. 1.

Similarly to the sound speed, the ratio p/ϵ is deeply connected to the principle of causality, which requires that the velocity of causal influences should not exceed the speed of

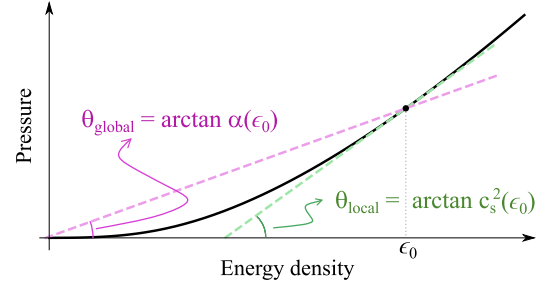


Figure 1: Geometrical interpretation of α (resp., c_s^2) as a global (resp., local) notion of the stiffness of nuclear matter. While $c_s^2(\epsilon_0)$ governs the change in pressure caused by an infinitesimal increment in energy density around $\epsilon = \epsilon_0$, $\alpha(\epsilon_0)$ determines the total increase in pressure from $\epsilon \approx 0$ (at the stellar surface) up to $\epsilon = \epsilon_0$ (say, at the stellar center).

light. For a perfect fluid, with energy-momentum tensor

$$T^{\mu\nu} = (\epsilon + p)u^\mu u^\nu + pg^{\mu\nu}, \quad (4)$$

where u^μ is the four-velocity of fluid elements, the adiabatic sound speed determines the propagation speed of sound waves, and causality then implies that [29]

$$c_s \leq 1. \quad (5)$$

On the other hand, the dominant energy condition (DEC)—which is the statement that the current of energy-momentum density, $-T^\mu_\nu \xi^\nu$, as measured by observers with four-velocity ξ^μ , should be future-directed or null—implies, for a perfect fluid (4), that $\epsilon \geq |p|$, or

$$\alpha \leq 1. \quad (6)$$

For a fluid characterized by a conserved energy-momentum tensor, the DEC implies that matter cannot travel faster than light, as it can be shown that if $T^{\mu\nu}$ vanishes on a close, achronal set S , it also vanishes in the domain of dependence of S (see lemma 4.3.1 in [30]). Therefore, condition (6) is also a statement about causal behavior of the fluid¹.

Of course, since in the nonrelativistic limit nuclear matter satisfies $p \ll \epsilon \approx \rho$, for the bound $\alpha = 1$ to be achieved, the fluid must first go superluminal; Eq. (5) is therefore more restrictive than (6). In particular, it is interesting to consider the case of an EOS that is “maximally soft”, $p(\epsilon) = 0$, for $\epsilon \leq \epsilon_0$, and “maximally stiff”, $p(\epsilon) = \epsilon - \epsilon_0$, for $\epsilon \geq \epsilon_0$, which yields the most compact NS models [33]. The maximally compact configuration, with $C \approx 0.35$, has $\epsilon_c = 3.024\epsilon_0$ and $p_c = 2.034\epsilon_c$ and therefore

$$\alpha_c = 0.670. \quad (7)$$

¹ Note that it is in principle possible to construct special Lorentz invariant (causal) theories that violate both Eqs. (5) and (6) [31, 32].

As we will see below, by requiring that the EOS satisfies Eq. (5), the bound (7) is approached, rather than (6).

Another relevant value for the stiffness measure (3) is $\alpha = 1/3$. Since $T \equiv g_{\mu\nu}T^{\mu\nu} = (3\alpha - 1)\epsilon$ for a perfect fluid, $\alpha = 1/3$ corresponds to $T = 0$. Again, for the value $\alpha = 1/3$ to be reached inside a NS, the conformal bound $c_s^2 < 1/3$ [34] must necessarily be violated in its interior. Notably, it has been pointed out before that the stellar compactness at which $T = 0$ at the stellar center is roughly EOS-independent [35]. This can be seen as a particular case of the more general, EOS-insensitive relation between the NS compactness and any specific value of α_c , which we now discuss.

III. SPACE OF EQUATIONS OF STATE

In order to explore the relation between α_c and macroscopic properties of NSs, we consider both a set of 25 realistic EOS and a set of 60,000 phenomenological EOS following two different parametrization schemes. The realistic EOS are derived from nuclear physics models under a variety of approximation schemes (see Appendix A of Ref. [36] for references and details). They are all hadronic except for QHC19 [37], which allows for a quark core. Here, we will use the parametrized form of these realistic EOS as described in Ref. [27] (cf. Table III of that reference). The set of phenomenological EOS comprises $\sim 30,000$ (generalized) piecewise polytropic EOS with continuous speed of sound [27] and $\sim 30,000$ spectral EOS [28]. In this section we briefly describe these parametrizations, as well as the properties of the final set of EOS.

In the generalized piecewise polytropic (GPP) parametrization developed in Ref. [27], one defines density intervals $\rho_0 < \rho_1 < \rho_2 < \dots$ above a certain value ρ_0 , in such a way that

$$p(\rho) = K_i \rho^{\Gamma_i} + \Lambda_i, \quad \rho_{i-1} \leq \rho \leq \rho_i. \quad (8)$$

The energy density $\epsilon(\rho)$ can be obtained from (8) and the first law of thermodynamics. This generalizes the usual piecewise polytropic parametrization (see, e.g. Ref. [38]) by introducing the parameters Λ_i , which can be adjusted in order to guarantee continuity of the speed of sound. One disadvantage of this construction is that Γ_i does not coincide with the adiabatic index (2) in each polytropic phase, rendering its interpretation less natural. Here, following Ref. [27], we fix the crust to the SLy(4) EOS [39], and divide the core into three density intervals, with dividing densities $\rho_1 = 10^{14.87} \text{ g/cm}^3$ and $\rho_2 = 10^{14.99} \text{ g/cm}^3$. Four free parameters define the EOS, which can be taken as K_1 and Γ_i , $i \in \{1, 2, 3\}$, while the remaining ones are determined by continuity and differentiability requirements.

We generate $\sim 30,000$ EOS by randomly sampling GPP parameters in the ranges $\Gamma_i \in [-2.0, 8.0]$. For each value of Γ_1 , $\log K_1$ is randomly sampled in the interval

$[\log K_{\min}(\Gamma_1), \log K_{\max}(\Gamma_1)]$, where $K_{\min/\max}$ are determined by the requirement that the density ρ_0 that divides crust and core satisfies $\rho_{\text{SLy}} < \rho_0 < \rho_1$, where $\rho_{\text{SLy}} = 5.317 \times 10^{11} \text{ g/cm}^3$ is the last dividing density for a GPP parametrization of the crust (see Table II of Ref. [27]). We further require that all accepted EOS (i) are causal, in the sense that Eq. (5) holds for all hydrodynamically stable configurations, and (ii) predict a maximum NS mass of at least $2.0M_\odot$, allowing for systems such as J0740+6620 [40]. We further assess the impact of setting an upper limit on the tidal deformability of a $1.4M_\odot$ NS, adopting the GW170817 constraint (iii) $\bar{\Lambda}_{1.4M_\odot} < 800$ [8]. For each accepted EOS, we generate 50 equilibrium configurations with central densities between ρ_{SLy} and that corresponding to the solution with maximum mass (ρ_{\max}). For the analyses in the following section, we restricted attention to configurations with $C > 0.05$.

In order to analyze the effect of a change to the EOS parametrization, we also consider the spectral parametrization presented in Ref. [28]. In this set-up the EOS is obtained as a solution to the differential equation

$$\frac{d\epsilon(p)}{dp} = \frac{\epsilon + p}{p \Gamma_1(p)}, \quad (9)$$

where the adiabatic index $\Gamma_1(p)$ is expanded as

$$\Gamma_1(p) = \exp \left[\sum_{k=0}^3 \gamma_k \left[\log \left(\frac{p}{p_0} \right) \right]^k \right]. \quad (10)$$

Here γ_k are free parameters specifying the EOS and p_0 is a reference pressure that determines the initial condition $\epsilon_0 \equiv \epsilon(p_0)$ for the integration of Eq. (9). It is defined as the pressure at the dividing density, chosen as $\rho_0 = 2 \times 10^{14} \text{ g/cm}^3$, between the low density EOS, which we take to be SLy [39], and the high density (core) EOS. The pressure at ρ_0 can be found from the definition (2) of the adiabatic index.

In principle, one could generate spectral EOS by directly sampling the parameters γ_k . However, we have found this procedure to be inefficient, since the adiabatic index is very sensitive to small changes in γ_k due to the exponential factor in Eq. (10), easily giving rise to nonphysical EOS. Instead, we have performed a random-walk in the EOS space, starting from the SLy parameters γ_k^{SLy} that can be found in Ref. [28]. Parameters for EOS i are such that $\gamma_k^i = \gamma_k^{i-1} + r_k^i \gamma_k^{\text{SLy}}$, where $\gamma_k^0 = \gamma_k^{\text{SLy}}$ and r_k^i are sampled uniformly in the interval $[-0.05, 0.05]$. In sampling the space of spectral EOS, we enforced conditions (i)-(iii) above, requiring causality, a $2.0M_\odot$ lower bound on the maximum mass, and an upper bound on the tidal deformability of a $1.4M_\odot$ NS ($\bar{\Lambda}_{1.4M_\odot} < 800$). Following this procedure, we generated $\sim 30,000$ EOS; for each one, 50 equilibrium configurations were computed from a minimum compactness of ~ 0.05 and up to the central density ρ_{\max} of the maximum-mass configuration.

EOS	Relation	a_0	a_1	a_2	a_3	a_4	a_5
Realistic	$\alpha_c - C$	-4.3997	27.754	-144.38	541.86	-10.295×10^2	857.16
	$\alpha_c - \bar{I}$	23.768	-38.842	24.44	-7.8292	1.245	-78.265×10^{-3}
	$\alpha_c - \bar{\Lambda}$	85.901×10^{-3}	-58.019×10^{-2}	82.016×10^{-3}	-10.5109×10^{-3}	6.967×10^{-4}	-1.8214×10^{-5}
Phenomenological (GPP)	$\alpha_c - C$	-4.619	33.734	-221.791	10.389×10^2	-24.278×10^{-3}	2173.6
	$\alpha_c - \bar{I}$	18.705	-29.445	17.655	-5.4557	84.167×10^{-2}	-51.543×10^{-3}
	$\alpha_c - \bar{\Lambda}$	-77.943×10^{-3}	-43.034×10^{-2}	27.195×10^{-3}	-16.601×10^{-4}	4.2749×10^{-5}	-9.4932×10^{-8}

Table I: Fit coefficients to the $\alpha_c - C/\bar{I}/\bar{\Lambda}$ relations, for a set of 25 realistic EOS (upper rows), and a set of 30,000 phenomenological (GPP) EOS (bottom rows).

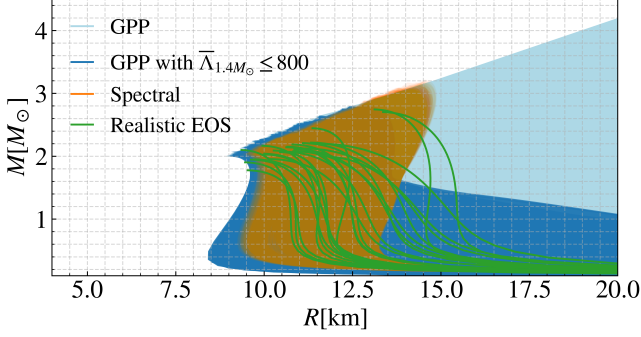


Figure 2: Mass-radius diagram for our set of 25 realistic EOS and 60,000 phenomenological EOS, of which half follow the GPP parametrization and half follow the spectral representation. The subset of GPP EOS obeying $\bar{\Lambda}_{1.4M_\odot} < 800$ is highlighted to allow for a clearer comparison with the spectral set, for which this condition also holds.

Figure 2 shows the final set of EOS. We see that, although the spectral set contains EOS with large maximum masses ($> 3.0M_\odot$) and largely accommodates the behavior of realistic EOS, it is still centered around the SLy EOS. On the other hand, the random sampling of GPP parameters allows for a much larger region of the EOS space to be covered with less samples. In what follows, we will use the set of 30,000 GPP EOS as our standard set.

IV. APPROXIMATE UNIVERSALITY

Here we explore the relation between the stiffness measure $\alpha_c = p_c/\epsilon_c$ and the NS compactness, moment of inertia and tidal deformability, for different choices of realistic or phenomenological EOS. The NS compactness, $C = M/R$, is computed from its mass M and radius R , obtained by numerically solving the TOV equations for spherically symmetric hydrostatic equilibrium. The NS moment of inertia, $I = J/\Omega$, is computed from its angular momentum J and angular velocity Ω in the approximation of slow rotation [41]. From it we construct the dimensionless quantity $\bar{I} = I/M^3$, which is known

to obey an EOS-insensitive relation with C [42]. Finally, the tidal deformability is computed by considering quadrupolar perturbations to an isolated NS; it measures the strength of the quadrupole moment Q_{ij} induced in a NS by an external tidal field \mathcal{E}_{ij} : $Q_{ij} = -\Lambda\mathcal{E}_{ij}$ [43–45]. Again, we consider its dimensionless version, $\bar{\Lambda} = \Lambda/M^5$, which is also known to obey an EOS-insensitive relation with C and \bar{I} [46]. In order to quantify the approximate universality of the $\alpha_c - C/\bar{I}/\bar{\Lambda}$ relations, we consider fifth-order polynomial fits of the form

$$\ln \alpha_c = \sum_{j=0}^5 a_j O^j, \quad (11)$$

where $O \in \{C, \ln \bar{I}, \ln \bar{\Lambda}\}$. The coefficients a_j for the set of realistic and phenomenological (GPP) EOS are given in Table I. Note that these fits can be optimized when some other property of a NS (such as its mass) is known.

Results for the set of 25 realistic EOS are shown in Fig. 3, together with fits of the form (11) and the corresponding fractional errors. For low compactness ($C \lesssim 0.2$), the $\alpha_c - C$ relation holds to a relative error of less than 4%, but the error increases for higher values of C , up to a maximum of $\sim 11\%$. Similarly, the universality of the $\alpha_c - \bar{I}/\bar{\Lambda}$ relations is stronger for larger values of \bar{I} and $\bar{\Lambda}$, and slightly weaker for lower values: The $\alpha_c - \bar{I}$ relation holds to a maximum error of $\sim 11\%$, while the $\alpha_c - \bar{\Lambda}$ relation holds to a maximum error of $\sim 8\%$ for this set of realistic EOS.

To further probe the approximate universality of the $\alpha_c - C/\bar{I}/\bar{\Lambda}$ relations, we explore a set of phenomenological EOS (cf. Sec. III). Figure 4 shows the $\alpha_c - C/\bar{I}/\bar{\Lambda}$ relations for a set of $\sim 30,000$ GPP EOS, together with fits of the form (11) and the corresponding fractional errors. The maximum value of α_c generated in this set of equilibrium solutions was ~ 0.662 , lower than the bound (7). For this set of EOS, the $\alpha_c - C$ relation holds to a maximum error of $\sim 57\%$, with 90% of errors below $\sim 18\%$; the $\alpha_c - \bar{I}$ relation holds to a maximum error of $\sim 41\%$, with 90% of errors below $\sim 8\%$; and the $\alpha_c - \bar{\Lambda}$ relation holds to a maximum error of $\sim 38\%$, with 90% of errors below $\sim 8\%$. These errors are much lower than those displayed by other relations linking macroscopic and microscopic properties (as we discuss in Sec. IV A below),

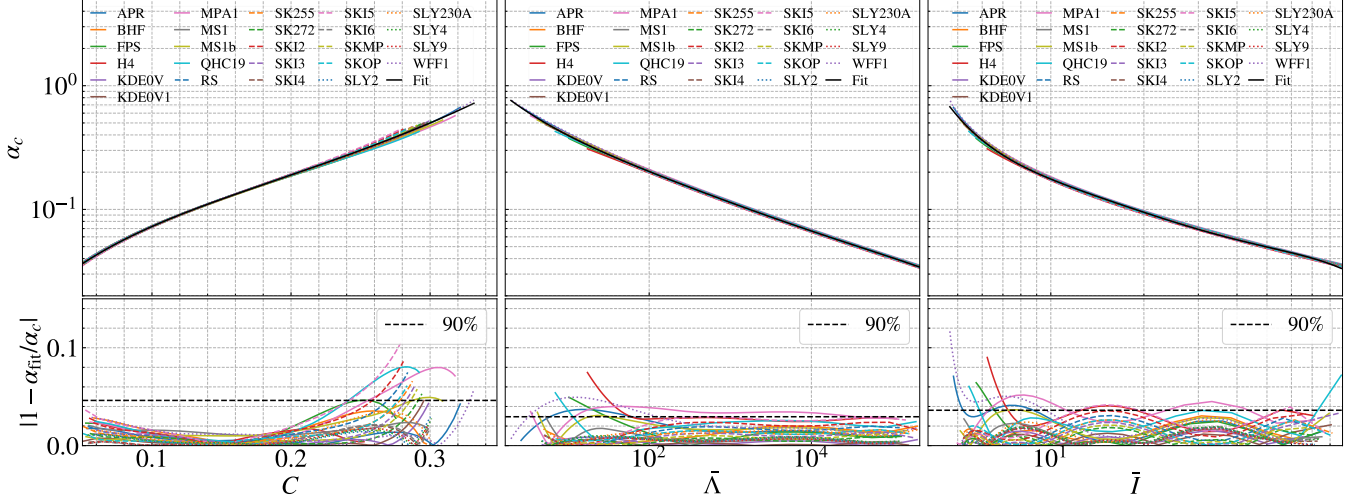


Figure 3: Approximately universal $\alpha_c - C/\bar{I}/\bar{\Lambda}$ relations for a set of 25 realistic EOS. A black line represents a fifth order polynomial fit [as in Eq. (11)], and the bottom panels display the corresponding fractional error. Only configurations with $C > 0.05$ are considered.

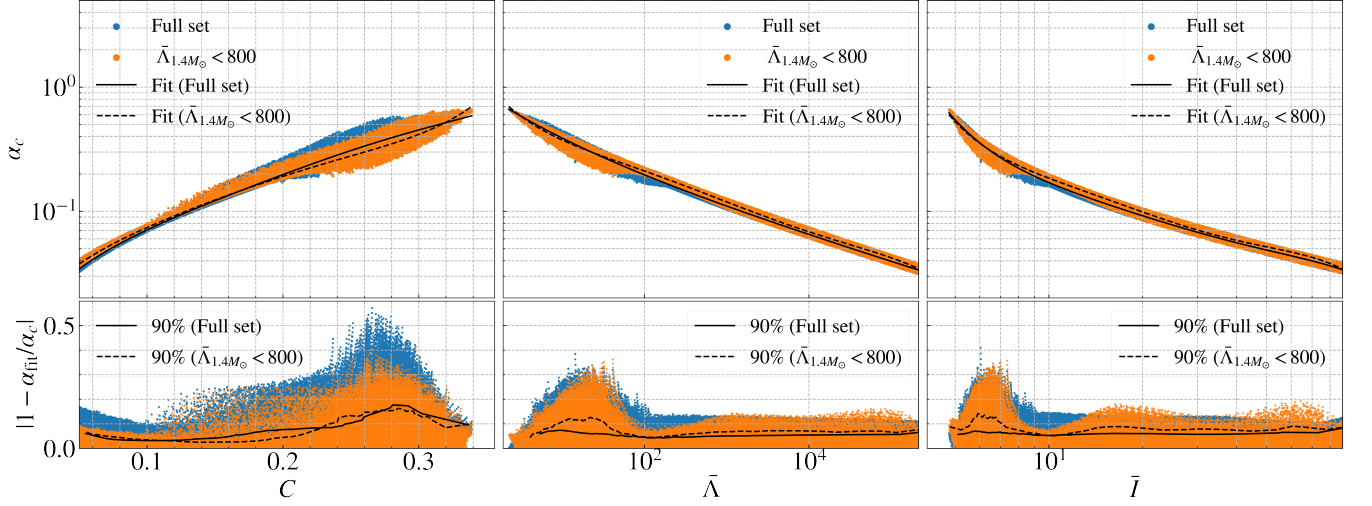


Figure 4: Approximately universal $\alpha_c - C/\bar{I}/\bar{\Lambda}$ relations for a set of $\sim 30,000$ phenomenological EOS in the GPP parametrization (blue), and for the subset obeying the additional requirement that $\bar{\Lambda}_{1.4M_\odot} < 800$ (orange). A solid (resp., dashed) black curve represents a fifth order polynomial fit [cf. Eq. (11)] to the full (resp., restricted) set of EOS. Bottom panels display the corresponding fractional error, with lines enclosing 90% of the errors. Only configurations with $C > 0.05$ are displayed.

and are comparable with those exhibited by some universal relations between macroscopic observables (such as between the quadrupole and higher multipoles of the tidal deformability [47, 48]). It is worth mentioning that roughly 30% of the GPP EOS in our set display an important softening at high densities, in such a way the speed of sound is not a monotonically increasing function of ρ (up to ρ_{\max}). These EOS contribute significantly to the larger spread seen in Fig. 4 for high values of C (or low \bar{I} , $\bar{\Lambda}$).

Finally, Fig. 5 compares the $\alpha_c - C/\bar{I}/\bar{\Lambda}$ relations for the set of GPP and spectral EOS. The trend is similar, but a smaller

region is covered by the set of spectral EOS. This is expected from the discussion in Sec. III since, for a fixed number of EOS, a random sampling of GPP parameters allows for a larger diversity of EOS behaviors than the random walk performed in the space of spectral EOS.

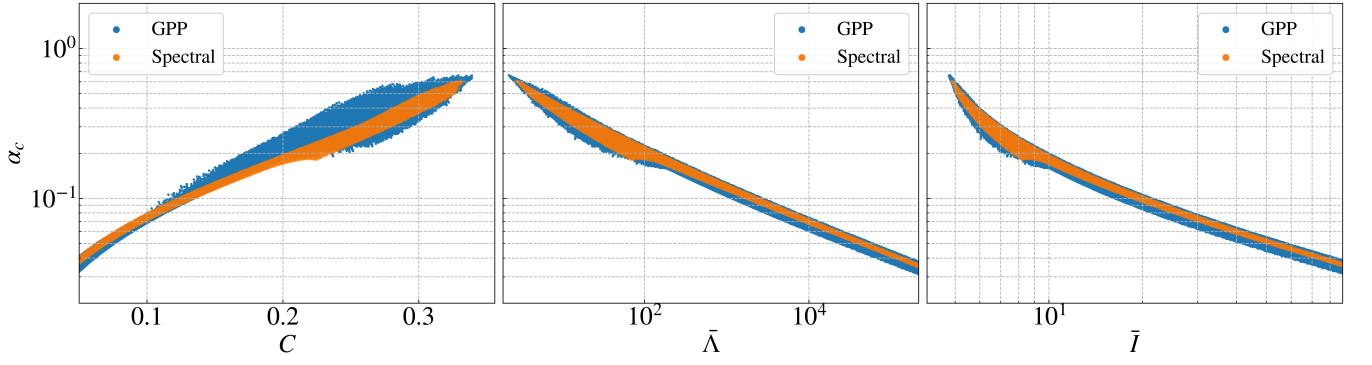


Figure 5: Universal $\alpha_c - C/\bar{I}/\bar{\Lambda}$ relations for a set of $\sim 30,000$ phenomenological EOS with the GPP parametrization (blue), and for $\sim 30,000$ EOS with the spectral parametrization (orange). Only configurations with $C > 0.05$ are displayed.

A. Comparison to other relations between macroscopic and microscopic quantities

To conclude this section, it is worthwhile to discuss how the $\alpha_c - C/\bar{I}/\bar{\Lambda}$ relations compare with other relations between macroscopic and microscopic NS properties.

First, it is interesting to stress that although α shares some properties with the speed of sound, as discussed in Sec. II, the correlation that is seen between α_c and $C/\bar{I}/\bar{\Lambda}$ is much weaker for, say, the sound speed at the stellar center ($c_{s,c}$). This is evident from Fig. 6, where the $\alpha_c - \bar{\Lambda}$ and $c_{s,c}^2 - \bar{\Lambda}$ relations are shown.

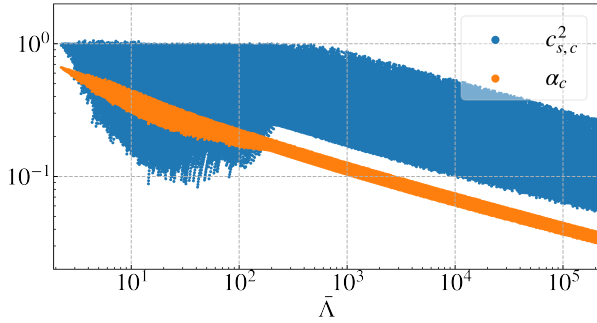


Figure 6: The ratio $\alpha_c = p_c/\epsilon_c$ and the square of the speed of sound at the stellar center, $c_{s,c}^2$, are shown as a function of $\bar{\Lambda}$ for a collection of equilibrium configurations obeying a set of $\sim 30,000$ phenomenological (GPP) EOS.

Second, we compare the $\alpha_c - C/\bar{I}/\bar{\Lambda}$ relations with the EOS-independent relation uncovered by Lattimer and Prakash, who showed that the radius of a NS with fixed mass (or, equivalently, its compactness) correlates well with the pressure around nuclear saturation density [22]. As a consequence of the Love-C (and I-C) relations [42, 46], a similar correlation is expected between the dimensionless tidal deformability (or moment of inertia) and pressure at $1-2\rho_{\text{sat}}$ (see, e.g., Ref. [23] for the case of the tidal deformability). This is illustrated for a

$1.4M_\odot$ NS in the first row of Fig. 7 for a set of GP (gray) and realistic (orange) EOS. The correlation is stronger for realistic EOS, but much weaker for the larger set of phenomenological EOS.

Now, around nuclear saturation density, the ratio ϵ/ρ between energy density and rest mass density is not expected to differ appreciably from unity — indeed, for the set of $\sim 30,000$ GPP EOS, $1.03 \lesssim \epsilon(2\rho_{\text{sat}})/(2\rho_{\text{sat}}) \lesssim 1.42$. As a consequence, a similar correlation is expected between $\alpha(1-2\rho_{\text{sat}})$ and the radius (or compactness, tidal deformability and moment of inertia) of a NS with fixed mass. This is shown in the second row of Fig. 7, which essentially mimics the first.

One might thus wonder whether the $\alpha_c - C/\bar{I}/\bar{\Lambda}$ relations we report in our work might be an extrapolation of the well-known relation of Lattimer and Prakash for the higher densities present in the NS core. The plots on the third row of Fig. 7 show, on the other hand, that the correlation between α and $R_{1.4M_\odot}$, $C_{1.4M_\odot}$ and $\bar{\Lambda}_{1.4M_\odot}$ is much stronger at the stellar center than around ρ_{sat} . Thus, it seems more robust to suggest that the $\alpha_c - C/\bar{I}/\bar{\Lambda}$ relations are more fundamental — in the sense of a weaker dependence on the EOS — and universality deteriorates when extended to lower densities. Still, it is worth noticing that x-ray observations and GW170817 constraints favor values of $R_{1.4M_\odot} < 15$ km, for which the scatter in the relations to α_c is somewhat larger.

V. CONNECTING TO OBSERVATIONS

The nearly universal relations presented in this work enable a relatively precise determination of the pressure to energy-density ratio at the core of a NS given a precise measurement of either C , $\bar{\Lambda}$ or \bar{I} . To demonstrate this, in this section we determine the posterior distribution for α_c for three NSs with recently measured properties: The primary and secondary components of event GW170817, for which the tidal deformability has been measured [9], and the massive pulsar J0740+6620, with mass $2.08 \pm 0.07M_\odot$ (68.3% credibility) [40], which re-

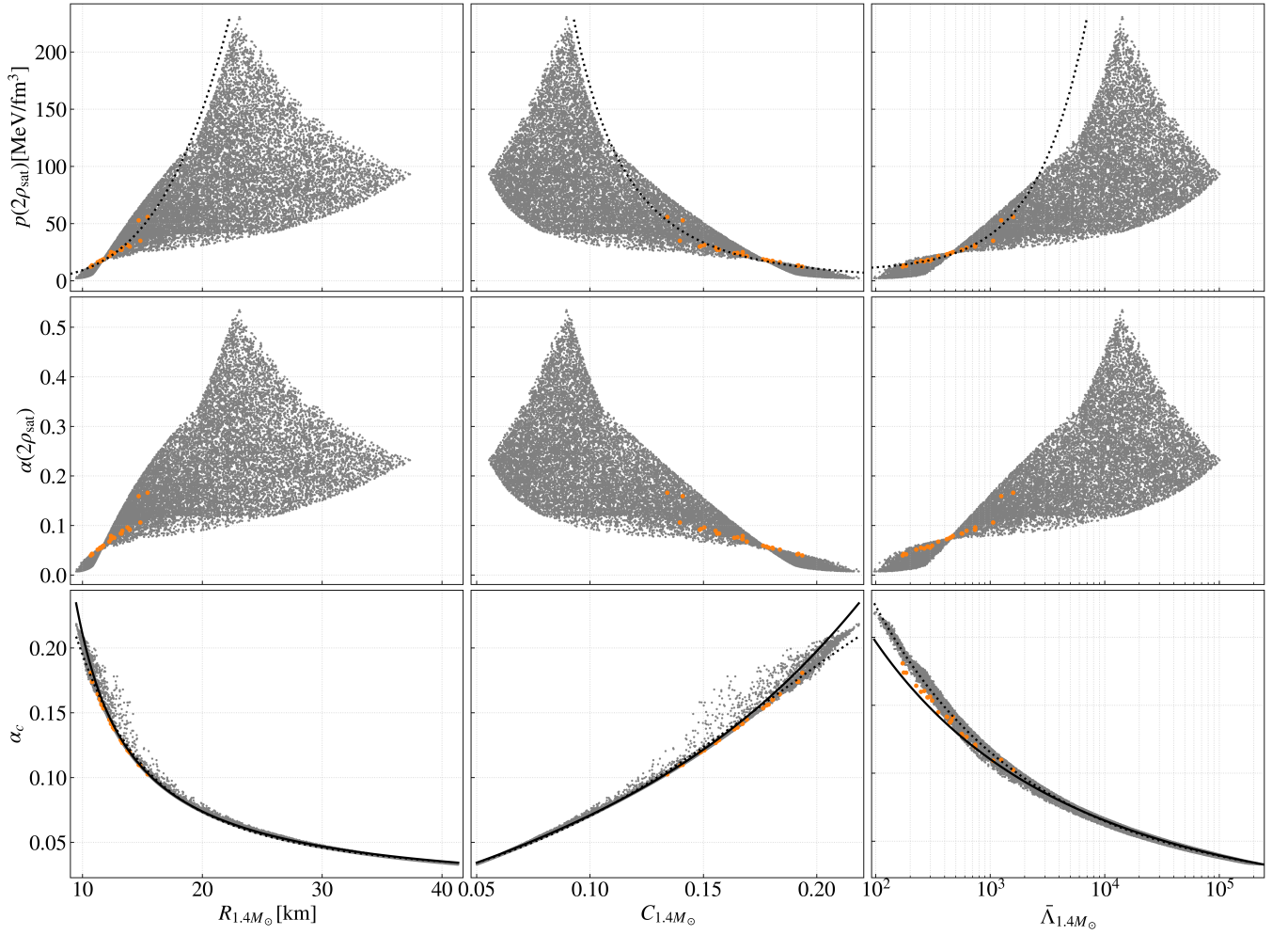


Figure 7: Top row: pressure at twice nuclear saturation density as a function of radius, compactness and dimensionless tidal deformability of a $1.4M_{\odot}$ NS for a set of GPP (gray) and realistic (orange) EOS. A black dotted line represents the fitting formulas $p(2\rho_{\text{sat}})^{-1/4}R_{1.4M_{\odot}} = 5.72 \text{ km MeV}^{-1/4} \text{ fm}^{3/4}$ [22] (first panel), $p(2\rho_{\text{sat}})^{1/4}C_{1.4M_{\odot}} = 0.361 \text{ MeV}^{1/4} \text{ fm}^{-3/4}$, which is a rescaling of the first (second panel), and $\bar{\Lambda}_{1.4M_{\odot}} = 31.59 p(2\rho_{\text{sat}})/(\text{MeV fm}^{-3}) - 272.36$ [23] (third panel). Middle row: same as first row, but for α at twice nuclear saturation density. Bottom row: same as first row, but for α_c . Solid black lines represent the fitting formulas from Table I, derived for the full set of stellar configurations (in the GPP parametrization), while dotted lines represent second order polynomial fits for this restricted set (with $M = 1.4M_{\odot}$); explicitly, they represent $\ln \alpha_c = -30.704 C^2 + 18.959 C - 4.2432$ (from which one obtains the fitting formula for $R_{1.4M_{\odot}}$) and $\ln \alpha_c = 73.308 \times 10^{-4} \ln \bar{\Lambda}^2 - 0.37 \ln \bar{\Lambda} + 47.688 \times 10^{-3}$. Only configurations with $C > 0.05$ are shown.

cently had its radius measured [6, 7]. Although NICER observations of pulsar J0030+0451 have also enabled estimates of its mass and radius [4, 5], we do not consider this NS in our analysis, since its $\sim 1.4M_{\odot}$ mass falls in the same range as the binary components that originated GW170817. Next, we explore how these posteriors would change given more precise measurements of NS properties.

Instead of basing our analysis on the fitting formulas presented in Table I, here we perform a full Bayesian analysis, as we describe below. The reason not to use the fitting formulas—especially in the case of broad experimental likelihoods—is that they do not carry information about the

underlying EOS distribution, which may have little or no support in some regions of parameter space.

In what follows, we compute $p(\alpha_c|\vec{D}, I)$, the posterior probability for α_c given some measurement of NS properties \vec{D} and background information I , by marginalizing $p(\alpha_c, \vec{\theta}|\vec{D}, I)$ over EOS parameters (in the GPP parametrization) $\vec{\theta} = \{\log K_1, \Gamma_1, \Gamma_2, \Gamma_3\}$. In practice, the marginalization is performed via Monte Carlo integration,

$$p(\alpha_c|\vec{D}, I) = \int d\vec{\theta} p(\alpha_c, \vec{\theta}|\vec{D}, I) \approx \frac{V_{\text{EOS}}}{N} \sum_{i=1}^N p(\alpha_c, \vec{\theta}_i|\vec{D}, I),$$

and we use as the set of N randomly sampled EOS parameters

$\vec{\theta}_i$ the same set generated for the previous analyses. The ranges for these parameters were described in Sec. III and define the volume V_{EOS} .

The probability $p(\alpha_c, \vec{\theta} | \vec{D}, I)$ that a star with properties \vec{D} has a given value α_c of central pressure to central energy density and EOS parameters $\vec{\theta}$ is computed from Bayes theorem,

$$p(\alpha_c, \vec{\theta} | \vec{D}, I) = \mathcal{N} p(\vec{D} | \alpha_c, \vec{\theta}, I) p(\alpha_c, \vec{\theta} | I), \quad (12)$$

where \mathcal{N} is a normalization factor that can be determined *a posteriori*. The prior $p(\alpha_c, \vec{\theta} | I)$ can be factored as $p(\alpha_c, \vec{\theta} | I) = p(\alpha_c | \vec{\theta}, I) p(\vec{\theta} | I)$. We assume the prior $p(\vec{\theta} | I)$ on the GPP EOS coefficients to be uniform in the ranges discussed in Sec. III, and $p(\alpha_c | \vec{\theta}, I)$ to be uniform in the range $\alpha(\rho_{\text{SLy}}) \leq \alpha_c \leq \alpha(\rho_{\text{max}})$, where ρ_{max} is the central density for the most massive NS predicted by an EOS with parameters $\vec{\theta}$. The likelihood $p(\vec{D} | \alpha_c, \vec{\theta}, I)$ is either inferred from publicly available experimental distributions or assumed to be Gaussian. In computing this likelihood, one has to take into account the fact $\alpha(\rho)$ may not be a monotonically increasing function of ρ in the range of interest, so that the inverse relation may not be single-valued.

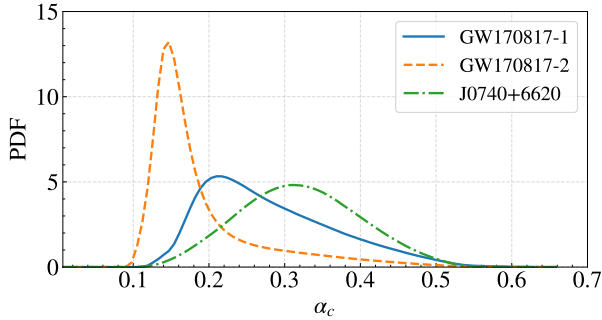


Figure 8: Posteriors for α_c for the primary (1) and secondary (2) components of the GW170817 event, as well as for pulsar J0740+6620.

Figure 8 shows the posterior probability density function (PDF) for α_c for the primary and secondary components of the binary NS system that originated GW170817, as well as for pulsar J0740+6620. For the components of the binary system, we only use information about their tidal deformabilities ($\vec{D} = \{\bar{\Lambda}\}$) [9], while for pulsar J0740+6620, we use information about its compactness ($\vec{D} = \{C\}$), computed from the mass and radius distributions obtained with NICER-only data by the group of Miller et al. [6].

The spread in the PDFs in Fig. 8 is determined by both measurement uncertainties and the residual EOS dependence of the $\alpha_c - C/\bar{\Lambda}$ relations. In order to explore the effect of increasing experimental precision (e.g. by third-generation GW detectors [49]), in Fig. 9 we show the posteriors for α_c given hypothetical observational likelihoods. The hypothetical measurement of observable O is assumed to follow a truncated ($O > 0$) Gaussian distribution with mean μ_O and variance

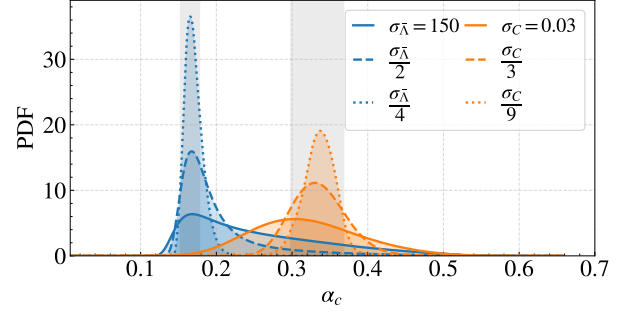


Figure 9: Posteriors for α_c given a hypothesized measurement of NS compactness (with mean $\mu_C = 0.26$; in blue) or dimensionless tidal deformability (with mean $\mu_{\bar{\Lambda}} = 200$; in orange). A truncated normal distribution with decreasing variance is assumed, starting with $\sigma_C = 0.03$ or $\sigma_{\bar{\Lambda}} = 150$. Gray vertical bands indicate 90% credible intervals centered at the median for the underlying distribution for α_c , inferred from Fig. 4.

σ_O^2 . In Fig. 9, $\mu_C = 0.26$ and $\mu_{\bar{\Lambda}} = 200$ and the standard deviation decreases from the initial values $\sigma_C = 0.03$ and $\sigma_{\bar{\Lambda}} = 150$, which are roughly compatible with GW170817 and J0740+6620 measurements. Initially, measurement uncertainties are the dominant source of error, but, as the measurement precision increases, the uncertainty in the posteriors eventually becomes dominated by the residual EOS dependence of the $\alpha_c - C/\bar{\Lambda}$ relations, which establish a lower bound for error bars (90% credible interval) at 0.165 ± 0.013 (for $\bar{\Lambda} = 200$) and 0.33 ± 0.03 (for $C = 0.26$). This relatively small uncertainty ($\lesssim 10\%$) is a manifestation of the approximate universality of the $\alpha_c - C/\bar{\Lambda}$ relations, and contrasts with the much larger uncertainties obtained for other microscopic quantities — for the same value of C (resp. $\bar{\Lambda}$), the underlying distribution for $c_{s,c}^2$ has a median and 90% credible interval of 0.66 ± 0.19 (resp. 0.35 ± 0.22).

VI. CONCLUSIONS

In this work we have uncovered approximately universal relations between certain NS observables (such as its compactness, moment of inertia and tidal deformability) and the pressure to energy-density ratio at the center of that NS, which can be interpreted as a measure of the mean stiffness of nuclear matter inside that object (cf. Sec. II). Figures 3 and 4 show our main results concerning the EOS-independence of the $\alpha_c - C/\bar{\Lambda}$ relations, which are stronger than other known relations linking macroscopic and microscopic properties (cf. Sec. IV A).

It is remarkable that a microscopic quantity characterizing the core of a NS may be reasonably recovered from a single, sufficiently precise measurement of a NS property

(cf. Sec. V); the approximately universal $\alpha_c - C/\bar{I}/\bar{\Lambda}$ relations presented here may thus provide a window into the extremeness of nuclear matter inside NSs. Additionally, these relations may be useful in tests of GR. Scalar extensions of GR – including models with cosmological applications such as the chameleon [50] or symmetron [51] – are known to predict a different phenomenology with respect to GR for NSs with $\alpha_c > 1/3$ [52–57]. Interestingly, Fig. 8 shows that the posterior for pulsar J0740+6620 has a significant support ($\sim 43\%$ probability) in the $\alpha_c > 1/3$ region, although the precise value varies somewhat for different data sets, such as those provided by Ref. [7] or when XMM-Newton data is included in the

analysis. In any case, the strong correlation between α_c and $C/\bar{I}/\bar{\Lambda}$, together with more precise NS measurements, should enable the identification of systems (if these do exist in Nature) where the condition on $\alpha_c > 1/3$ is likely satisfied, opening a new window for tests of modified theories of gravity.

ACKNOWLEDGMENTS

This work was partially supported by the National Council for Scientific and Technological Development (CNPq), and by the Carlos Chagas Filho Research Support Foundation (FAPERJ).

-
- [1] M. Kramer, I. H. Stairs, R. N. Manchester, M. A. McLaughlin, A. G. Lyne, R. D. Ferdman, M. Burgay, D. R. Lorimer, A. Possenti, N. D’Amico, J. M. Sarkissian, G. B. Hobbs, J. E. Reynolds, P. C. C. Freire, and F. Camilo, Tests of general relativity from timing the double pulsar, *Science* **314**, 97 (2006).
 - [2] J. M. Weisberg, D. J. Nice, and J. H. Taylor, Timing measurements of the relativistic binary pulsar PSR B1913+16, *Astrophys. J.* **722**, 1030 (2010).
 - [3] E. Fonseca, I. H. Stairs, and S. E. Thorsett, A comprehensive study of relativistic gravity using PSR B1534+12, *Astrophys. J.* **787**, 82 (2014).
 - [4] M. C. Miller, F. K. Lamb, A. J. Dittmann, S. Bogdanov, Z. Arzoumanian, K. C. Gendreau, S. Guillot, A. K. Harding, W. C. G. Ho, J. M. Lattimer, R. M. Ludlam, S. Mahmoodifar, S. M. Morsink, P. S. Ray, T. E. Strohmayer, K. S. Wood, T. Enoto, R. Foster, T. Okajima, G. Prigozhin, and Y. Soong, PSR J0030+0451 mass and radius from NICER data and implications for the properties of neutron star matter, *Astrophys. J.* **887**, L24 (2019).
 - [5] T. E. Riley, A. L. Watts, S. Bogdanov, P. S. Ray, R. M. Ludlam, S. Guillot, Z. Arzoumanian, C. L. Baker, A. V. Bilous, D. Chakrabarty, K. C. Gendreau, A. K. Harding, W. C. G. Ho, J. M. Lattimer, S. M. Morsink, and T. E. Strohmayer, A NICER view of PSR J0030+0451: Millisecond pulsar parameter estimation, *Astrophys. J.* **887**, L21 (2019).
 - [6] M. C. Miller, F. K. Lamb, A. J. Dittmann, S. Bogdanov, Z. Arzoumanian, K. C. Gendreau, S. Guillot, W. C. G. Ho, J. M. Lattimer, M. Loewenstein, S. M. Morsink, P. S. Ray, M. T. Wolff, C. L. Baker, T. Cazeau, S. Manthripragada, C. B. Markwardt, T. Okajima, S. Pollard, I. Cognard, H. T. Cromartie, E. Fonseca, L. Guillemot, M. Kerr, A. Parthasarathy, T. T. Pennucci, S. Ransom, and I. Stairs, The radius of PSR J0740+6620 from NICER and XMM-Newton data, *Astrophys. J. Lett.* **918**, L28 (2021).
 - [7] T. E. Riley, A. L. Watts, P. S. Ray, S. Bogdanov, S. Guillot, S. M. Morsink, A. V. Bilous, Z. Arzoumanian, D. Choudhury, J. S. Deneva, K. C. Gendreau, A. K. Harding, W. C. G. Ho, J. M. Lattimer, M. Loewenstein, R. M. Ludlam, C. B. Markwardt, T. Okajima, C. Prescod-Weinstein, R. A. Remillard, M. T. Wolff, E. Fonseca, H. T. Cromartie, M. Kerr, T. T. Pennucci, A. Parthasarathy, S. Ransom, I. Stairs, L. Guillemot, and I. Cognard, A NICER view of the massive pulsar PSR J0740+6620 informed by radio timing and XMM-Newton spectroscopy, *Astrophys. J. Lett.* **918**, L27 (2021).
 - [8] B. P. Abbott, R. Abbott, T. D. Abbott, *et al.* (LIGO Scientific Collaboration and Virgo Collaboration), GW170817: Observation of Gravitational Waves from a Binary Neutron Star Inspiral, *Phys. Rev. Lett.* **119**, 161101 (2017).
 - [9] B. P. Abbott, R. Abbott, T. D. Abbott, *et al.* (The LIGO Scientific Collaboration and the Virgo Collaboration), GW170817: Measurements of neutron star radii and equation of state, *Phys. Rev. Lett.* **121**, 161101 (2018).
 - [10] B. P. Abbott, R. Abbott, T. D. Abbott, *et al.*, Multi-messenger observations of a binary neutron star merger, *Astrophys. J.* **848**, L12 (2017).
 - [11] M. Kramer and N. Wex, The double pulsar system: a unique laboratory for gravity, *Classical Quantum Gravity* **26**, 073001 (2009).
 - [12] J. Clark, A. Bauswein, L. Cadonati, H.-T. Janka, C. Pankow, and N. Stergioulas, Prospects for high frequency burst searches following binary neutron star coalescence with advanced gravitational wave detectors, *Phys. Rev. D* **90**, 062004 (2014).
 - [13] H. Yang, V. Paschalidis, K. Yagi, L. Lehner, F. Pretorius, and N. Yunes, Gravitational wave spectroscopy of binary neutron star merger remnants with mode stacking, *Phys. Rev. D* **97**, 024049 (2018).
 - [14] A. Torres-Rivas, K. Chatziioannou, A. Bauswein, and J. A. Clark, Observing the post-merger signal of GW170817-like events with improved gravitational-wave detectors, *Phys. Rev. D* **99**, 044014 (2019).
 - [15] J. M. Lattimer and M. Prakash, The equation of state of hot, dense matter and neutron stars, *Phys. Rep.* **621**, 127 (2016).
 - [16] F. Özel and P. Freire, Masses, radii, and the equation of state of neutron stars, *Annu. Rev. Astron. Astrophys.* **54**, 401 (2016).
 - [17] K. Yagi and N. Yunes, Approximate universal relations for neutron stars and quark stars, *Phys. Rep.* **681**, 1 (2017).
 - [18] K. Yagi and N. Yunes, Binary love relations, *Classical Quantum Gravity* **33**, 13LT01 (2016).
 - [19] K. Yagi and N. Yunes, Approximate universal relations among tidal parameters for neutron star binaries, *Classical Quantum*

- Gravity **34**, 015006 (2017).
- [20] K. Yagi and N. Yunes, I-Love-Q: Unexpected universal relations for neutron stars and quark stars, *Science* **341**, 365 (2013).
 - [21] K. Yagi and N. Yunes, I-Love-Q relations in neutron stars and their applications to astrophysics, gravitational waves, and fundamental physics, *Phys. Rev. D* **88**, 023009 (2013).
 - [22] J. M. Lattimer and M. Prakash, Neutron star structure and the equation of state, *Astrophys. J.* **550**, 426 (2001).
 - [23] Y. Lim and J. W. Holt, Neutron star tidal deformabilities constrained by nuclear theory and experiment, *Phys. Rev. Lett.* **121**, 062701 (2018).
 - [24] F. Özel and D. Psaltis, Reconstructing the neutron-star equation of state from astrophysical measurements, *Phys. Rev. D* **80**, 103003 (2009).
 - [25] J. M. Lattimer and A. W. Steiner, Constraints on the symmetry energy using the mass-radius relation of neutron stars, *Eur. Phys. J. A* **50**, 40 (2014).
 - [26] C. Drischler, J. Holt, and C. Wellenhofer, Chiral effective field theory and the high-density nuclear equation of state, *Annu. Rev. Nucl. Part. Sci.* **71**, 403 (2021).
 - [27] M. F. O’Boyle, C. Markakis, N. Stergioulas, and J. S. Read, Parametrized equation of state for neutron star matter with continuous sound speed, *Phys. Rev. D* **102**, 083027 (2020).
 - [28] L. Lindblom, Spectral representations of neutron-star equations of state, *Phys. Rev. D* **82**, 103011 (2010).
 - [29] A. M. Anile, *Relativistic Fluids and Magneto-fluids: With Applications in Astrophysics and Plasma Physics*, Cambridge Monographs on Mathematical Physics (Cambridge University Press, 1990).
 - [30] S. W. Hawking and G. F. R. Ellis, *The Large Scale Structure of Space-Time* (Cambridge University Press, 1973).
 - [31] S. A. Bludman and M. A. Ruderman, Possibility of the speed of sound exceeding the speed of light in ultradense matter, *Phys. Rev.* **170**, 1176 (1968).
 - [32] S. A. Bludman and M. A. Ruderman, Noncausality and instability in ultradense matter, *Phys. Rev. D* **1**, 3243 (1970).
 - [33] S. Koranda, N. Stergioulas, and J. L. Friedman, Upper limits set by causality on the rotation and mass of uniformly rotating relativistic stars, *Astrophys. J.* **488**, 799 (1997).
 - [34] P. Bedaque and A. W. Steiner, Sound velocity bound and neutron stars, *Phys. Rev. Lett.* **114**, 031103 (2015).
 - [35] D. M. Podkowka, R. F. P. Mendes, and E. Poisson, Trace of the energy-momentum tensor and macroscopic properties of neutron stars, *Phys. Rev. D* **98**, 064057 (2018).
 - [36] B. P. Abbott *et al.*, Model comparison from LIGO-Virgo data on GW170817’s binary components and consequences for the merger remnant, *Classical Quantum Gravity* **37**, 045006 (2020).
 - [37] G. Baym, S. Furusawa, T. Hatsuda, T. Kojo, and H. Togashi, New Neutron Star Equation of State with Quark-Hadron Crossover, *Astrophys. J.* **885**, 42 (2019).
 - [38] J. Read, B. Lackey, B. Owen, and J. L. Friedman, Constraints on a phenomenologically parametrized neutron-star equation of state, *Phys. Rev. D* **79**, 124032 (2009).
 - [39] F. Douchin and P. Haensel, A unified equation of state of dense matter and neutron star structure, *Astron. Astrophys.* **380**, 151 (2001).
 - [40] E. Fonseca, H. T. Cromartie, T. T. Pennucci, P. S. Ray, A. Y. Kirichenko, S. M. Ransom, P. B. Demorest, I. H. Stairs, Z. Arzoumanian, L. Guillemot, A. Parthasarathy, M. Kerr, I. Cognard, P. T. Baker, H. Blumer, P. R. Brook, M. DeCesar, T. Dolch, F. A. Dong, E. C. Ferrara, W. Fiore, N. Garver-Daniels, D. C. Good, R. Jennings, M. L. Jones, V. M. Kaspi, M. T. Lam, D. R. Lorimer, J. Luo, A. McEwen, J. W. McKee, M. A. McLaughlin, N. McMann, B. W. Meyers, A. Naidu, C. Ng, D. J. Nice, N. Pol, H. A. Radovan, B. Shapiro-Albert, C. M. Tan, S. P. Tendulkar, J. K. Swiggum, H. M. Wahl, and W. W. Zhu, Refined mass and geometric measurements of the high-mass PSR J0740+6620, *Astrophys. J. Lett.* **915**, L12 (2021).
 - [41] J. B. Hartle, Slowly Rotating Relativistic Stars. I. Equations of Structure, *Astrophys. J.* **150**, 1005 (1967).
 - [42] C. Breu and L. Rezzolla, Maximum mass, moment of inertia and compactness of relativistic stars, *Mon. Not. R. Astron. Soc.* **459**, 646 (2016).
 - [43] T. Hinderer, Tidal Love Numbers of Neutron Stars, *Astrophys. J.* **677**, 1216 (2008).
 - [44] T. Damour and A. Nagar, Relativistic tidal properties of neutron stars, *Phys. Rev. D* **80**, 084035 (2009).
 - [45] T. Binnington and E. Poisson, Relativistic theory of tidal Love numbers, *Phys. Rev. D* **80**, 084018 (2009).
 - [46] A. Maselli, V. Cardoso, V. Ferrari, L. Gualtieri, and P. Pani, Equation-of-state-independent relations in neutron stars, *Phys. Rev. D* **88**, 023007 (2013).
 - [47] K. Yagi, Multipole Love relations, *Phys. Rev. D* **89**, 043011 (2014).
 - [48] D. A. Godzieba, R. Gamba, D. Radice, and S. Bernuzzi, Updated universal relations for tidal deformabilities of neutron stars from phenomenological equations of state, *Phys. Rev. D* **103**, 063036 (2021).
 - [49] Z. Carson, A. W. Steiner, and K. Yagi, Future prospects for constraining nuclear matter parameters with gravitational waves, *Phys. Rev. D* **100**, 023012 (2019).
 - [50] J. Khoury and A. Weltman, Chameleon Fields: Awaiting Surprises for Tests of Gravity in Space, *Phys. Rev. Lett.* **93**, 171104 (2004).
 - [51] K. Hinterbichler and J. Khoury, Screening Long-Range Forces through Local Symmetry Restoration, *Phys. Rev. Lett.* **104**, 231301 (2010).
 - [52] R. F. P. Mendes and N. Ortiz, Highly compact neutron stars in scalar-tensor theories of gravity: Spontaneous scalarization versus gravitational collapse, *Phys. Rev. D* **93**, 124035 (2016).
 - [53] C. Palenzuela and S. L. Liebling, Constraining scalar-tensor theories of gravity from the most massive neutron stars, *Phys. Rev. D* **93**, 044009 (2016).
 - [54] B. F. de Aguiar and R. F. P. Mendes, Highly compact neutron stars and screening mechanisms: Equilibrium and stability, *Phys. Rev. D* **102**, 024064 (2020).
 - [55] G. Ventagli, A. Lehébel, and T. P. Sotiriou, Onset of spontaneous scalarization in generalized scalar-tensor theories, *Phys. Rev. D* **102**, 024050 (2020).
 - [56] A. Dima, M. Bezares, and E. Barausse, Dynamical chameleon neutron stars: Stability, radial oscillations, and scalar radiation in spherical symmetry, *Phys. Rev. D* **104**, 084017 (2021).
 - [57] B. F. de Aguiar, R. F. P. Mendes, and F. T. Falciano, Neutron Stars in the Symmetron Model, *Universe* **8**, 6 (2021).